PROGRESS IN COLOR, COLORANTS AND COATINGS

available online @ www.pccc.icrc.ac.ir

Prog. Color Colorants Coat. 14 (2021), 101-112

Ministry of Science, Research and Technology
Institute for Color Science and Technology

Investigating the Effects of Thickness on the Performance of ZnO-Based DSSC

E. Kouhestanian, M. Ranjbar*, S. A. Mozaffari, H. Salaramoli

Thin Layer and Nanotechnology Laboratory, Department of Chemical Technology, Iranian Research Organization for Science and Technology (IROST), P.O. Box: 33535-111, Tehran, Iran.

ARTICLE INFO

Article history:
Received: 25 Mar 2020
Final Revised: 27 Jun 2020
Accepted: 28 Jun 2020
Available online: 15 Sept 2020

Keywords:
Dye-sensitized solar cell
Electrochemical impedance spectroscopy
Photo-anode thickness
Thickness effect
ZnO nanoparticles.

ABSTRACT

Zinc oxide nanostructures exhibit unique properties which make them suitable for dye-sensitized solar cell applications. Their specific properties such as appropriate optical properties, proper energy band gap and high electron transfer characteristics have motivated researchers to use them in the fabrication of dye-sensitized solar cell photo-anodes. In the present study, the effect of thickness on the performance of a new ZnO photo-anode has been studied. All the photovoltaic parameters of the cells fabricated using N719 ruthenium dye were measured. SEM technique was utilized to determine the thickness and the UV-Visible method was used to study the transparent properties of the photo-anodes. Electrochemical impedance spectroscopy technique was employed to determine the appropriate equivalent circuit for studying the electron transfer mechanisms in all the fabricated cells. The results demonstrated that the ZnO thickness is a critical parameter for providing either sufficient resistance to suppress the charge recombination process or appropriate electron transferring properties. The optimized ZnO photo-anode was obtained at a thickness of 19 µm, which resulted in an efficiency of 3.22%. Prog. Color Colorants Coat. 14 (2021), 101-112© Institute for Color Science and Technology.

1. Introduction

Dye-Sensitized Solar Cells (DSSCs) are a new generation of solar cells which are considered to be an economically reliable alternative model for the previous solar cell technology [1, 2]. Because of their benefits, scientists have done much efforts to improve the DSSCs efficiency [3, 4]. Since the semiconductor oxides in various nanostructures are the main part of DSSC photo-anodes, developing a new semiconductor is the subject of current scientific studies. Although TiO_2 nanostructures are the first candidate for DSSC photo-anodes, the unique characteristics of ZnO nanostructures, such as excellent electron mobility (200 cm^2V^{-1} s^{-1}), which is greatly larger than that of TiO_2 nanostructures (30 cm^2V^{-1} s^{-1}), superior energy band gap, and higher electron transfer characteristics, make them an appropriate alternative semiconductor for DSSC applications [5, 6]. Also, the synthesis of ZnO nanostructures is more controllable than that of TiO_2 nanostructures. This is an important factor in various applications, particularly in solar cell technology [7-9].

In spite of the above-mentioned benefits, the general yield of ZnO-based DSSCs is less than that of TiO_2. The maximum efficiency obtained for pure ZnO dye-sensitized solar cell is in the range of about 6-8 %, as reported by various research groups [10-12], which

*Corresponding author: marandjbar@irost.ir

is almost half of the highest efficiency reported for TiO_2-based DSSCs [13]. Some literatures reported the effect of dye sensitization mechanism on the DSSC efficiency, especially for ZnO photo-anodes [14, 15]. Generally, dye sensitization step is an important process in cell fabrication via various techniques. Initially, dye molecules are adsorbed on the surface of photo-electrode after diffusion into the porous network. Meanwhile, it is possible for dye molecules to collide in the pores of the film. In the case of ZnO, diffusion and adsorption is associated with the dissolution of surface Zn atoms by the protons released from the dye molecules in an ethanol solution, leading to the formation of Zn2*p*/dye complex and the decrease in the ZnO stability in acidic solution. So, it causes a dominate negative effect in cell performance and reduces the cell efficiency [16, 17]. Due to these facts, controlling the critical parameters such as dye composition, concentration, solvent, pH and immersion time is important to achieve high efficiency ZnO-based DSSCs.

On the other hand, according to the literature [18, 19], the rate constant of electron injection from commercial acidic ruthenium-based dyes, like N719, into ZnO nanostructures is significantly slower (more than 100 times) as compared to TiO_2 nanostructures. The TiO_2 conduction band is principally consisted of unoccupied 3d orbitals from Ti4*p* while the ZnO nanostructure conduction bands are derived mainly from the unoccupied s and p orbitals of Zn2*p*. So, this difference in ZnO band structure, which is caused by the variety of density of states and probably different electronic coupling strengths with dye molecules, resulted in insufficient electron injection. Hence, the synthesis of new sensitized dyes appropriate for ZnO-based DSSCs has attracted the attention of researchers [20, 21]. Various ZnO nanostructures have been applied to fabricate photo-anodes. In traditional DSSCs, the porous photo-anodes are consisted of two kinds of nanoparticles with approximately 20-30 nm in diameter and submicron-sized particles act as transparent and scattered layers, respectively. The transparent layer affords a large interfacial surface area for both dye adsorption and electron transfer, while the submicron-sized particles either can be mixed with the nanocrystalline film [22, 23] or deposited on top of the nanocrystalline film [24, 25]. So, it provides a light scattering layer to create efficient electron transfer processes. The function of both transparent and scattering layers is schematically shown in Figure 1.

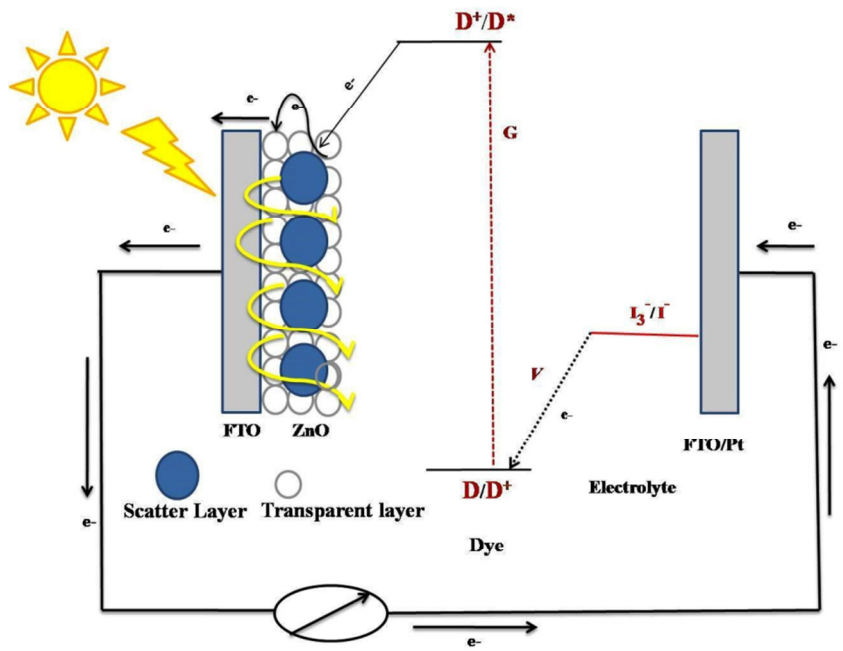

Figure 1: Illustration of charge transfer processes occur on the FTO/ZnO photo-anode with dye/electrolyte interface in dye-sensitized solar cells. *G* (molcm^{-2} s^{-1}) indicates the electron excitation rate; *V* represents the reaction rate between oxidized dye and iodide (mol cm^{-2} s^{-1}).

Recently, we synthesized 30 and 350 nm ZnO nanoparticles via sonochemical method in methanol and deionized water using supramolecule precursors [26]. The aim of this work is to study the effect of ZnO photo-anode thickness on the cell performance. Various techniques, including EIS method, were carried out to extract critical parameters to investigate the cell performance. In addition, a new ZnO nanocomposite paste was prepared as our innovation. The synthesized ZnO nanoparticles with 30 and 350 nm particle sizes as transparent and scattering were mixed by the ratio of 3:1. Moreover, we achieved the maximum efficiency by optimizing the ZnO photo-anode thickness. In fact, photo-anode thickness is a critical parameter in cell fabrication. The optimum thickness depends on the nanoparticle size, paste composition, deposition and modification techniques [27].

Furthermore**,** all the photovoltaic parameters were studied for the ZnO-based DSSCs fabricated using N719 Ruthenium dye. Electrochemical impedance spectroscopy was employed to determine the electron lifetime, charge transfer and charge transport resistance values at the ZnO/electrolyte interfaces by using a suggested equivalent circuit model**.**

2. Experimental

2.1. Materials and apparatus

All chemicals were of analytical grade and were used without further purification. $ZnCl_2$, 2,6-pyridinediamine = [pyda], 2,6-pyridinedicarboxylic acid = [pydc.H_2] (Aldrich), N719 dye and FTO (Fluorinated Tin Oxide) glass sheets with 15 Ωcm^{-2} resistances were supplied from Solaronix S.A. Co. The electrolyte solution in acetonitrile (Iodolyte ELT-ACN-I Sharif Solar, Iran) was purchased from Sharif Solar Co. Moreover, a multiwave ultrasonic generator (UP600S, Mosonix) was used for ultrasonic irradiation equipped with a converter/transducer and titanium oscillator (horn), 12.5 mm in diameter, operating at 20 kHz with a maximum power output of 600 W. The ultrasonic generator automatically adjusts the power level. A potentiostat/galvanostat apparatus (PGSTAT. 302N, Autolab, Eco-Chemie, The Netherlands) was used to do cyclic voltammetry (CV), and electrochemical impedance spectroscopy (EIS) tests. The photocurrent-voltage (I-V) curves were measured using the potentiostat/galvanostat apparatus at 100 $mWcm^{-2}$ and air mass 1.5 G illumination by a simulated sunlight equipment SIM10 model. A Hitachi S4160 FE-SEM instrument was used to study the surface and the thickness of the nanolayers. The UV-Visible spectroscopy (Perkin-Elmer) was performed to study the transparent properties of the ZnO layers.

2.2. Preparation of ZnO nanocomposite paste

40 wt% of ZnO nanoparticles with the particle sizes of 30 and 350 nm were dispersed in ethanol with the ratio of 3:1 by sonication and stirring. ZnO composite paste was obtained according to Ito method [24] by mixing 80 wt% α terpineol and 10 wt% ethyl cellulose. The paste was ultrasonicated and stirred for 30 min to obtain a homogeneous mixture.

2.3. Preparation of ZnO photo-electrodes

The F-doped SnO_2 conducting glass substrates (FTO) were cleaned using ultrasonic bath (5 min in acetone, 5 min in alcohol), rinsed with water, treated by 45% nitric acid solution for 2 min before drying in nitrogen atmosphere [28], and finally used to make both the working and counter electrodes. Dr. Blade method was performed to deposit ZnO paste on FTO layers. In each step, the photo-anodes were dried for 15 min at 120 °C and employed again for coating the new layer. Finally, four photo-anodes from 1 to 4 layers were prepared and sintered gradually under airflow through a specific temperature program [24].

2.4. Fabrication of DSSCs

The ZnO photo-electrodes with the active area of 0.25 cm^2 were immersed in the dye solution containing 0.3 mM N719 at room temperature. Dye solution was prepared using a mixture of isopropanol/acetonitrile with the ratio of 1:1 as the solvent. The prepared photo-anode with one to four coated layers was immersed in dye solution for 0.5 to 2 h [28]. All photo-electrodes were rinsed with the prepared solvent and dried at room temperature to be used in cell fabrication. The counter electrodes were made by drop coating of 0.5 mM H_2PtCl_6 solution on the FTO surface and then heating for 15 min at 400 °C [29]. For assembling the cells, a thermal adhesive film (Surlyn, Dyesol, 30-µm-thick) was used to seal the cells by pressing the structure at 120 °C and finally, a drop of electrolyte solution (Iodolyte ELTACN- I Sharif Solar, Iran) was inserted into the cell via a hole, which was created at

the back of the counter electrode. Subsequently, the filled hole was sealed with a small glass.

3. Results and Discussion

As reported recently, one-pot synthesis by ultrasonic method at ambient temperature and atmospheric pressure was done to obtain the Zn(II) supramolecular by adding pyridine-2,6-diaminium pyridine-2,6-dicarboxylate (LH2) and $ZnCl_2$ with 1:2 mole ratio in both DI water and dry methanol solvents, separately. The effect of solvent on the synthesis method is studied and reported in perevious report [26]. The obtained precursors were annealed under the particular thermal procedure to prepare ZnO powders, which were finally used to make nanocomposite paste [26]. Figure 2 displays the image of the prepared ZnO layer prepared by Dr. Blade technique. The quasi-spherical shapes were formed via nanoparticle aggregation.

The presence of smaller particle size can afford a large surface area to adsorb dye molecules and transfer electrons into photo-anode. Indeed, the particles with approximately 200-400 nm sizes are utilized to reflect the transmissible incident light towards the ZnO photo-anode to improve the optical path of the incident light in the ZnO photo-anode [30, 31]. Furthermore, using approximately 350 nm ZnO spherical particles in composite photo-anode afford not only sufficient scattering light but also a large surface area to enhance the dye absorption. Therefore, preparing such nanocomposites provides a multifunctional material with both light-scattering and fast electron transport characteristics. Particle size distribution of these nanoparticles is reported in [26]. Moreover, quantitative analysis using energy-dispersive X-ray spectroscopy (EDX) was accomplished to investigate the chemical composition of the ZnO layer shown in Figure 3. The presence of silicon, tin, zinc, and fluorine was detected which was consistent with the previous studies [32].

To enhance the cell efficiency, the photo-anode thickness was varied by sequential deposition of 1 to 4 layers. The cross-section was analyzed by SEM to determine the Photo-anode thicknesses. The thicknesses were increased up to 24 micrometers (Figure 4). The previously reported thickness of the first layer was about 7 micrometers [26].

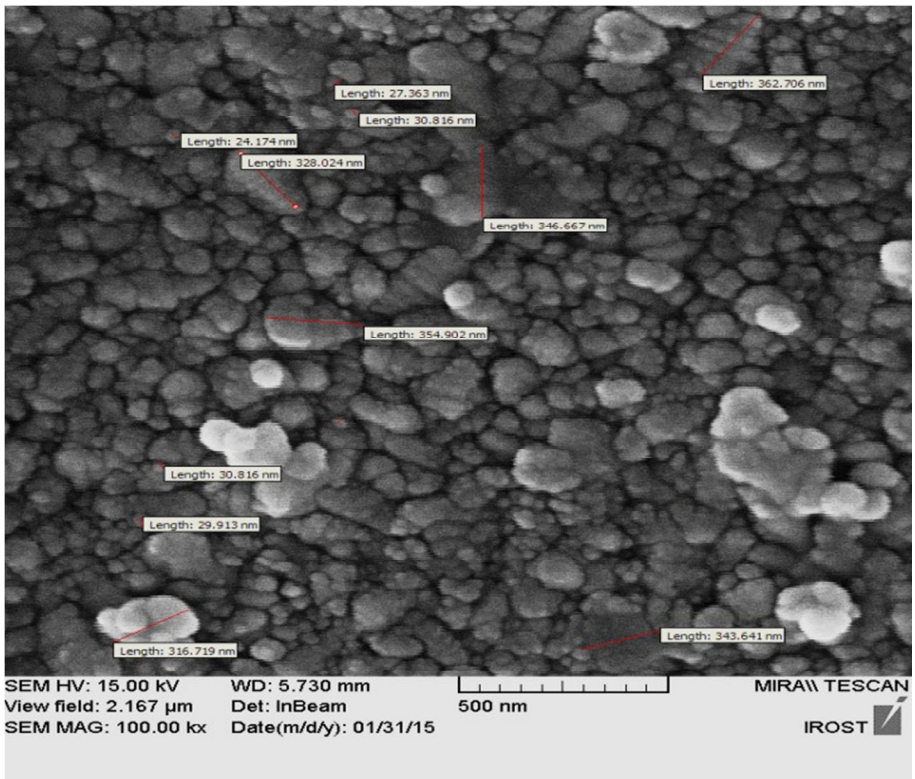

Figure 2: SEM image of ZnO photo-anode with one coated layer.

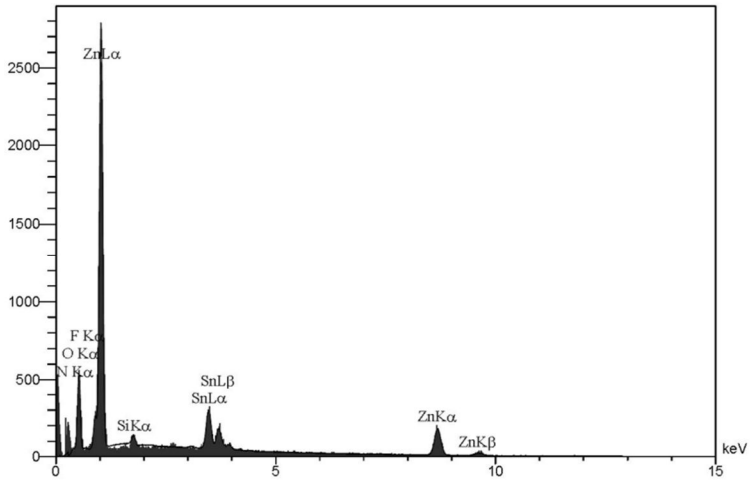

Figure 3: EDX spectrum of FTO/ZnO photo-anode with one coated layer.

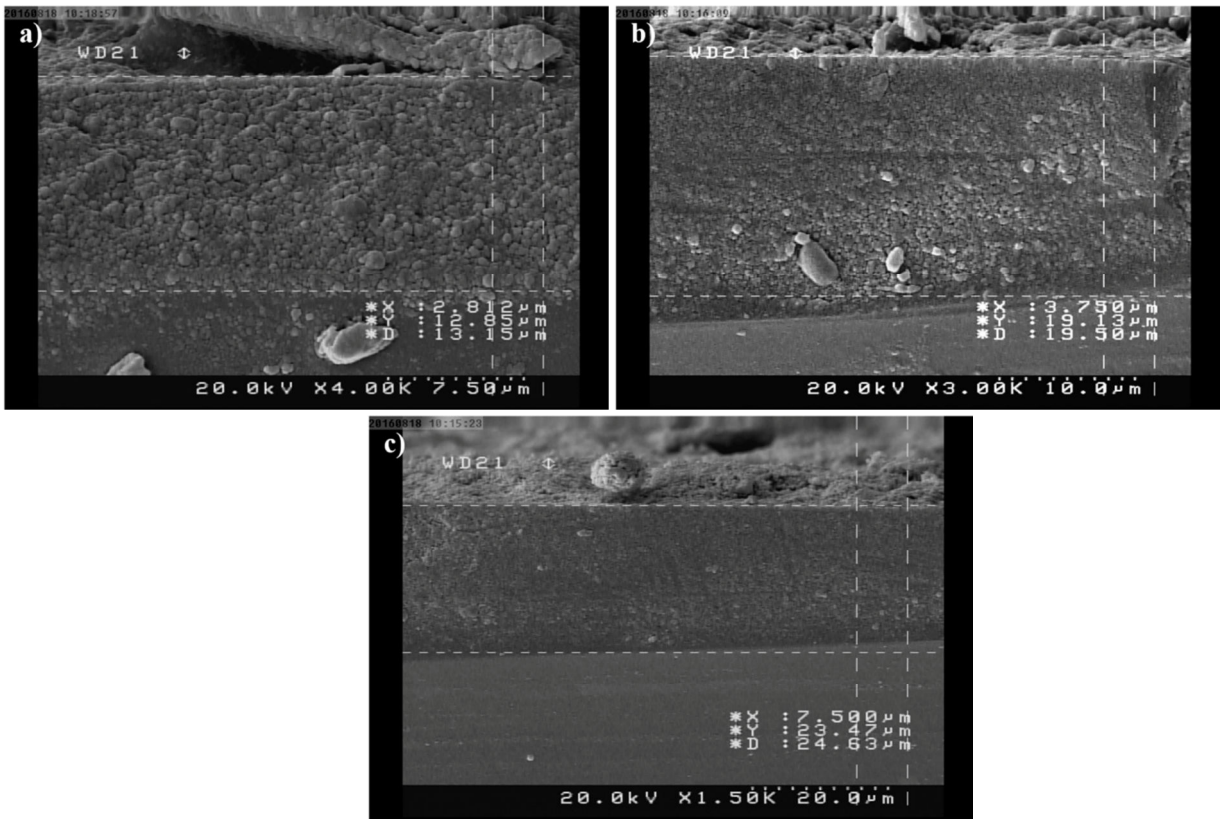

Figure 4: SEM images obtained from the cross-section of ZnO photo-anodes with: (a) two coated layers, (b) three coated layers and (c) four coated layers.

The transparency of prepared layers was also studied by UV-Visible technique (Figure 5). The prepared layers indicated proper transparency, which decreased with increasing the thickness from 1 to 4 layers. The transparency of the fourth layer decreased to less than 3%, which can explain the efficiency decline.

3.1. J-V characteristics and performance of DSSCs

In order to study the influence of photo-anode thickness on the performance of ZnO-based DSSCs, the current density-voltage (J-V) characteristic curves are plotted in Figure 6. Various photovoltaic

parameters of the fabricated cells are shown in Table 1. In fact, the amount of adsorbed dye, light absorption, and light scattering of ZnO particles increased by enhancing the total interfacial surface area of the porous film by increasing the film thickness. The short-current density (J_{SC}) values were improved due to the increasing of the film thickness and surface area [33, 34]. The open-circuit voltage (V_{OC}) values were also enhanced significantly which can demonstrate the effect of ZnO on retarding the recombination reactions.

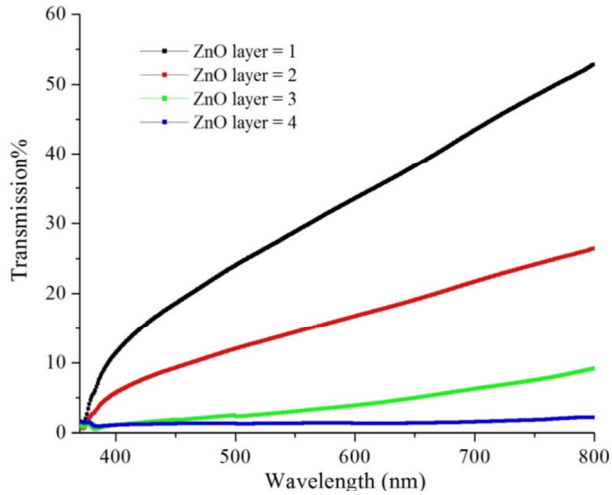

Figure 5: Transmittance spectra of ZnO photo-anode prepared from one to four coated layers.

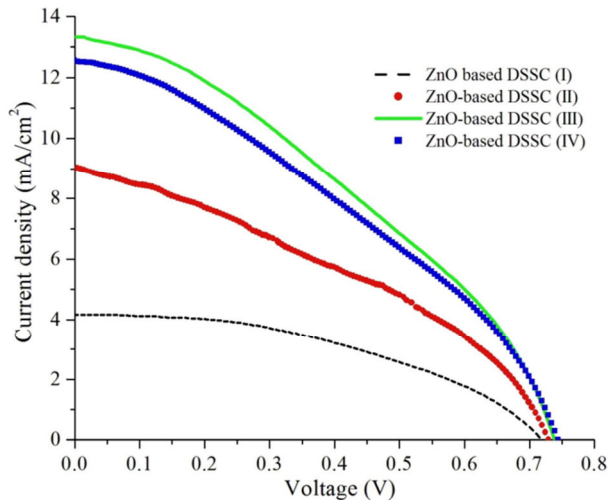

Figure 6: J-V characteristic curves of the ZnO-based DSSCs with various ZnO thicknesses.

Table 1: J-V characteristic curves for all the fabricated ZnO-based DSSCs prepared by different thicknesses of the photo-anodes from 1 to 4 coated layers.

No	No. of Deposited layers	Photoanode	Thickness (µm)	J_{sc} (mAcm^{-2})	V_{oc} (V)	FF	η (%)
I	1	ZnO	7.00	4.16	0.72	0.43	1.3
II	2	ZnO	13.15	8.11	0.73	0.36	2.15
III	3	ZnO	19.50	13.32	0.74	0.35	3.48
IV	4	ZnO	24.63	12.57	0.74	0.34	3.22

However, increasing the film thickness creates more restrictions on mass transfer, which enhances the overall resistance and finally has a dominant-negative result on the cell performance. Thus, the film thickness must be optimized to obtain efficient solar cells. The maximum efficiency was achieved at a thickness of 19 micrometers. The effect of ZnO thickness on the photovoltaic parameters of fabricated cells is depicted in Figure 7 (a-d).

It is notable that all photovoltaic parameters increase from one to three coated layers where a contradiction about FF values is recognized (Figure 7(c)). While by considering the direct relation between the efficiency and FF values, the same pattern in their variations is expected. The variation of FF values is due to overall resistance of cell including series including transport and recombination transfer resistances which are completely explained by EIS technique. Although the photo-anode 1 displays more FF value, the FF variation between photo-anode 2 and 3 is negligible and the maximum value of FF variation is about 0.1. Such contradiction is also notable in literature, especially when the thickness is studied and a new method or materials is used to modify the new photo-anode [35-37].

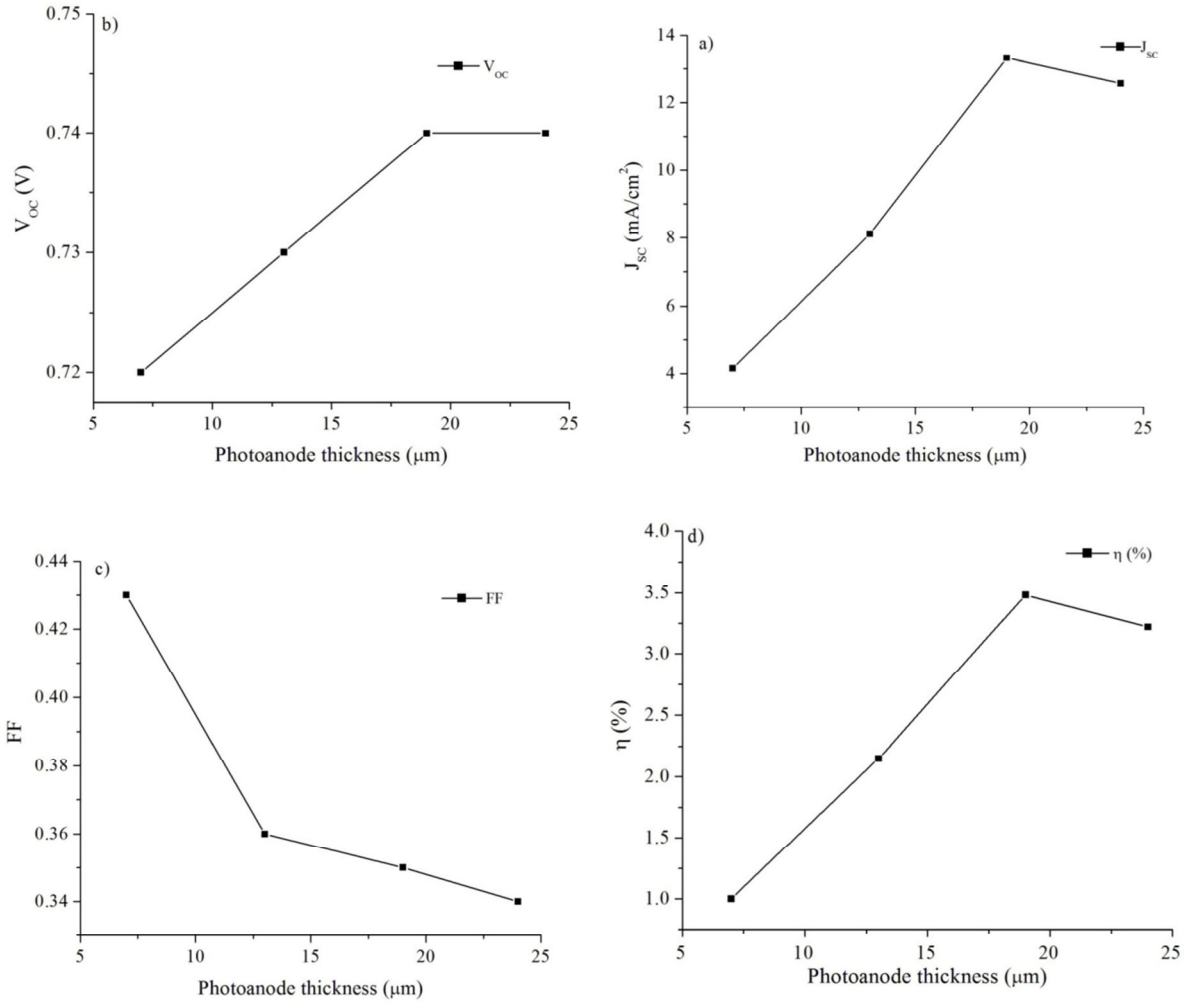

Figure 7: Variation of photovoltaic parameters of the fabricated ZnO DSSCs (a) J_{SC}, (b) V_{OC}, (c) *FF* and (d) η; with different deposited layers.

3.2. Electron transport and interfacial transfer properties

3.2.1. Linear sweep voltammetry

CV method is used to study the mechanism of interfacial electron transfer in DSSCs. The voltammetric behavior is mostly related to the distribution and density of local states and affords significant information. Under forward bias, cathodic current increases due to the reduction of I_3^- ions of the electrolyte via electrons injected from the FTO substrate toward the mesoporous semiconductor. In contrast, at the reverse bias, the voltammetric behavior corresponds to the regeneration reaction of dye molecules [38]. The cathodic current can afford information about the position of the electronic Fermi level (E_F) being close to the conduction band edge (E_{cb}). The forward bias is primarily attributed to the difference between the electronic Fermi level (E_F), and the redox potential of electrolyte (E_{redox}), where the value of E_{redox} is a constant value in the cell (Figure 8a). So, due to the relationship between the current and forward bias, the onset potential in cathodic current can identify the position of the conduction band edge of semiconductor (E_{cb}) [39]. The voltammetry curves of all the fabricated ZnO-based DSSC cells were performed in the dark at a scan rate of 50 mVs^{-1} from -1.0 to 1.0 V (Figure 8b). Furthermore, by increasing the number of coated layers, the onset potentials changed in cathodic current and under the forward bias. This is an indicative of the influence of ZnO thin film in shifting the conduction band position of semiconductor and decreasing the interfacial reaction of electrons with I_3^- ions. The current reduction under forward bias also exhibits the performance of ZnO thin film as an inherent energy barrier that significantly suppresses charge recombination reactions.

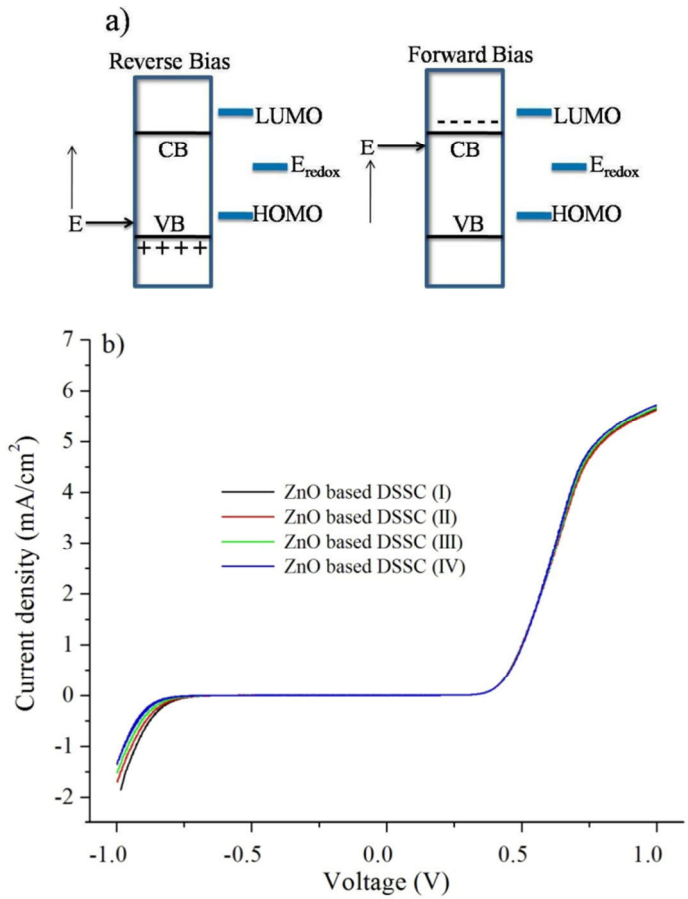

Figure 8: (a) A schematic diagram showing the interfacial charge transfer processes at dye-sensitized semiconductor electrode under forward and reverse bias, (b) Cyclic voltammograms of ZnO electrodeposition on FTO layer from 1.0 to -1.0 V versus saturated calomel electrode (SCE) as reference and Pt wire as counter electrode with 50 mVs^{-1} scan rates in the dark.

3.2.2. EIS study of the fabricated DSSCs

Electrochemical impedance spectroscopy (EIS) is a reliable, non-destructive and informative technique which is utilized to investigate the electrochemical and electrical characteristics of the interfaces [32, 40, 41]. In fact, EIS reveals the mechanism of the functional features of all DSSCs with various ZnO thicknesses. In order to gain an insight toward the interfacial charge transfer processes in the DSSCs, EIS was performed with an electrochemical workstation at $-V_{OC}$ bias (in V) at room temperature in dark conditions. The AC amplitude was set at 10 mV and the frequency was in the range of 100 kHz to 1 mHz.

The Nyquist, Figure 9(a), and Bode, Figure 9(b), plots of EIS spectra exhibit two main frequency peaks which are correlated to the charge behavior of ZnO-based DSSCs in various interfaces. Also, the maximum frequency peak (f_{max}) at mid-frequency range is due to the charge recombination process at ZnO electrodes. Zview/Zplot software (scribner Associates, Inc.) was utilized based on Macdonald's algorithm (LEVM 7) with a complex non-linear least square (CNLS) approximation method to make an equivalent circuit for fitting the measured EIS spectra. As shown in Figure 9(c), the equivalent circuit is consisted of two semicircles which illustrate the main interfaces in DSSC. The first semicircle which is associated with the high-frequency region (100 kHz-100 Hz) shows the resistance of electrolyte/Pt counter electrode interface ($R1=R_{Pt}$). The second semicircle is correlated to the intermediate frequency range (100Hz-1 Hz) which denotes the charge transport resistance (R_t) and charge transfer resistance (R_{ct}) at the photo-electrode/electrolyte interface. R_s corresponds the total resistance of the solution and the conducting glass sheet. Besides, the constant phase elements (*CPEs*), containing the two parameters of *CPE-T* and *CPE-P*, exhibit non-ideal capacitance in the semicircles.

All values of the equivalent circuit parameters were attained from the EIS plot via fitting data [42], as represented in Table 2. Effective lifetime (τ_{eff}) is an important factor which indicates the solar cell performance, and significantly depends on the recombination reactions. Indeed, the higher value of τ_{eff} represents the less recombination process. τ_{eff} can be measured by the EIS method by either Bode or Nyquist plots (eq. 3 and 4). f_{max} is the maximum frequency of the mid-frequency peak and ω_{max} is the maximum angular frequency of the impedance semicircle arc at medium frequencies. The results display that the values from both methods are in acceptable agreement with each other. Both R_{ct} and the chemical capacitance, C_{μ}, parameters can also be achieved from fitting the data of Nyquist plots to determine the τ_{eff} by equations 1 to 3, as reported in Table 2 [43].

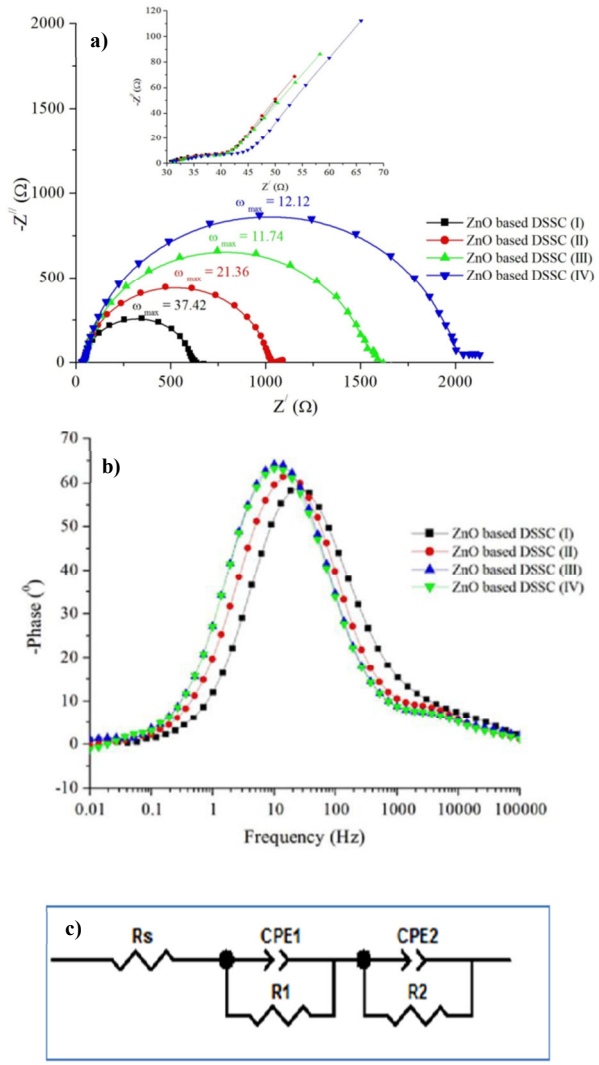

Figure 9: (a) EIS plots of fabricated DSSCs based on the various prepared photo-anodes. The inset represents the higher resolution of the straight line at high frequencies which accounts for electron transport in all photo-anodes; b) Bod plots of the prepared ZnO-based DSSC; and (c) equivalent circuit used for impedance data approximation where R_s, *R* and *CPE* represent the solution resistance, charge-transfer resistance, and constant-phase element, respectively.

Table 2: The values of the equivalent circuit parameters approximated from the EIS data obtained for all the fabricated cells.

#	R_s (Ω)	*CPE2-T* (Ω)	*CPE2-P* (Ω)	R_{ct} (Ω)	R_t (Ω)	R_{ct}/R_t	c_μ (Fcm^{-2})	*t* (ms) Eq. 3	*t* (ms) Eq. 4	L_n (μm)	*L* (μm)	$D_n \times 10^{-6}$ (cm^2s^{-1})
I	30.50	5.26×10^{-5}	0.95	575.21	6.28	91.59	4.37×10^{-5}	25.16	26	66.95	7.05	0.172
II	30.46	6.38×10^{-5}	0.94	973.10	8.10	120.13	5.34×10^{-5}	51.91	47	142.48	13.15	0.432
III	30.31	7.17×10^{-5}	0.93	1491.23	10.45	142.46	6.05×10^{-5}	90.33	85	226.77	19.50	0.604
IV	30.32	5.36×10^{-5}	0.93	1949.12	16.23	120.08	4.52×10^{-5}	88.15	82	262.99	24.63	0.843

$$\tau_{eff}=R_{ct}\times C_\mu \quad (1)$$

$$C_\mu=\frac{(R_{ct}\times \text{CPE-T})^{1/\text{CPE-P}}}{Rct} \quad (2)$$

$$\tau_{eff}=(R_{ct}\times \text{CPE-T})^{1/\text{CPE-P}} \quad (3)$$

$$\tau_{eff}=\frac{1}{\omega_{max}}=\frac{1}{2\pi f_{max}} \quad (4)$$

Since, the EIS technique allows one to obtain the recombination resistance, R_{rec}, and the transport resistance, R_{tr}, would be an efficient method to study the effect of photo-anode thickness for achieving the highest performance. According to the literature, the ratio of R_{ct}/R_{tr} is a significant parameter in determining the cell performance and is used to compare the performance of cells. In fact, the higher value of this ratio implies the higher efficiency of the cell. According to equation 5, the ratio of film thickness (L) to the electron diffusion length (L_n) is proportional to R_{ct}/R_{tr} ratio [44].

$$\frac{L_n}{L}=\left(\frac{R_{ct}}{R_{tr}}\right)^{1/2} \quad (5)$$

It is worth noting that the film thickness has an essential influence on the DSSC performance. The values of L_n (Eq. 6) for all the cells were measured and reported in Table 2. L_n displays the length of electron diffusion toward the anode before it is lost through recombination reactions. So, the diffusion length should be larger than the film thickness. The enhancement in L_n values indicate the lowest recombination reactions, and collection of the highest injected electrons on FTO layers [45, 46].

$$L_n=\sqrt{\tau_n D_n} \quad (6)$$

The chemical diffusion coefficients which can be used to introduce a cell performance were calculated by equation 6. Low diffusion coefficients are theoretically attributed to the presence of large number of trapped states. They are produced through the distortion of the crystal structure at grain boundaries, which enhance the scattering effects, surface area, and localized states at grain boundaries, all acting as electron traps [47].

4. Conclusion

In summary, this study reports the successful fabrication of ZnO based-DSSCs using synthesized ZnO nanoparticles as photo-anode. The effect of film thickness was systematically investigated. The EIS technique was performed to study the physical parameters of the fabricated cells. The results obtained from J-V and EIS tests are in satisfactory agreement with each other. These results are useful in obtaining the optimum photo-anode thickness. The results showed that to attain an efficient ZnO/N719-based DSSC, the photo-anode thickness should be optimized. Finally, a new ZnO-based DSSC with the efficiency of 3.22 % and the photo-anode thickness of 19 μm was achieved successfully.

Acknowledgments

Author acknowledges the support rendered by the Iranian Research Organization for Science and Technology (IROST), Iran Nanotechnology Initiative Council (INIC), and Sharif Solar Co. for this research.

5. References

1. J. Khan, M. H. Arsalan, Solar power technologies for sustainable electricity generation-A review, *Renew. Sustain. Energy Rev.*, 55(2016), 414-425.
2. J. Gong, K. Sumathy, Q. Qiao, Z. Zhou, Review on dye-sensitized solar cells (DSSCs): Advanced techniques and research trends, *Renew. Sustain. Energy Rev*., 68(2017), 234-246.
3. S. A. Kazmi, S. Hameed, A. S. Ahmed, M. Arshad, A. Azam, Electrical and optical properties of graphene-TiO_2 nanocomposite and its applications in dye sensitized solar cells (DSSC). *J. Alloys and Compd*., 691(2017), 659-665.
4. A. Hegazy, N. Kinadjian, B. Sadeghimakki, S. Sivoththaman, N. K. Allam, E. Prouzet, TiO_2 nanoparticles optimized for photoanodes tested in large area dye-sensitized solar cells (DSSC), *Sol. Energy. Mater. Sol. Cells*, 153(2016), 108-116.
5. C. Y. Lin, Y. H. Lai, H. W. Chen, J. G. Chen, C. W. Kung, R. Vittal, K. C. Ho, Highly efficient dye-sensitized solar cell with a ZnO nanosheet-based photoanode, *Energy Environ. Sci*., 4(2011), 3448-3455.
6. M. U. Rahman, M. Wei, F. Xie, M. Khan, Efficient dye-sensitized solar cells composed of nanostructural ZnO doped with Ti, *Catalysts,* 9(2019), 273-284.
7. T. Marimuthu, A. K. Narayanasamy, T. Rangasamy, S. Surya, Facile growth of ZnO nanowire arrays and nanoneedle arrays with flower structure on ZnO-TiO_2 seed layer for DSSC applications, *J. Alloy Compd*., 693(2017), 1011-1019.
8. Q. Zhang, C. Li, TiO_2 coated ZnO nanorods by mist chemical vapor deposition for application as photoanodes for dye-sensitized solar cells, *Nanomaterials,* 9(2019), 1339-1352.
9. S. Rasouli, Sh. Saket, One step rapid synthesis of nano-crystalline ZnO by microwave-assisted solution combustion method, *Prog. Color. Color. Coat*., 3(2010), 19-25.
10. Y. He, J. Hu, Y. Xie, High-efficiency dye-sensitized solar cells of up to 8.03% by air plasma treatment of ZnO nanostructures, *Chem. Commun*., 51(2015), 16229-16232.
11. M. Ye, X. Wen, M. Wang, J. Locozzia, N. Zhang, C. Lin, Z. Lin, Recent advances in dye-sensitized solar cells: from photoanodes, sensitizers and electrolytes to counter electrodes, *Mater. Today*, 18(2015), 155-162.
12. R. Vittal, K. C. HO, Zinc oxide dye-sensitized solar cells: A review, *Renew. Sustain. Energy Rev*., 70(2017), 920-935.
13. S. Mathew, A. Yella, P. Gao, R. Humphry-Baker, B. E. F. Curchod, N. Ashari-Astani, I. Tavernelli, U. Rothlisberger, M. Khaja Nazeeruddin, M. Grätzel, Dye-sensitized solar cells with 13% efficiency achieved through the molecular engineering of porphyrin sensitizers, *Nature Chem*., 6(2014), 242-247.
14. S. S. Khadtare and H. M. Pathan, Rose bengal sensitized ZnO photoelectrode for dye sensitized solar cell: optimizing the performance, *J. Renew. Sustain. Energy*, 6(2014), 053131-053138.
15. K. Premaratne, G. R. A. Kumara, R. M. G. Rajapakse, M. L. Karunarathne, Highly efficient, optically semi-transparent, ZnO-based dye-sensitized solar cells with indoline D -358 as the dye, *J. Photochem. Photobiol. A: chem*., 229(2012), 29-32**.**
16. A. B. F. Martinson, T. W. Hamann, M. J. Pellin, J. T. Hupp, New architectures for dye-sensitized solar cells, *Chem. Eur. J*., 14(2008), 4458-4467.
17. C. C. Raj, R. Prasanth, A critical review of recent developments in nanomaterials for photoelectrodes in dye sensitized solar cells. *J. Power Sources*, 317(2016), 120–132.
18. J. Han, F. Fan, C. Xu, S. Lin, M. Wei, X. Duan, Z. L. Wang, ZnO nanotube-based dye-sensitized solar cell and its application in self-powered devices, *Nanotechnology*, 21(2010), 405203-405209.
19. K. Keis, C. Bauer, G. Boschloo, A. Hagfeldt, K. Westermark, H. Rensmo, H. Siegbahn, Nanostructured ZnO electrodes for dye-sensitized solar cell applications, *J. Photochem. Photobiol. A: chem*., 148(2002), 57-64.
20. G. S. Selopal, H. P. Wu, J. Lu, Y. Chang, M. Wang, A. Vomiero, I. Concina, E. W. G. Diau, Metal-free organic dyes for TiO_2 and ZnO dye-sensitized solar cells, *Scientific Reports*, 6(2016), 18756- 18767.
21. J. Patwari, S. Shyamal, T. Khan, H. Ghadi, C. Bhattacharya, S. Chakrabarti, S. K. Pal, Inversion of activity in DSSC for TiO_2 and ZnO photo-anodes depending on the choice of sensitizer and carrier dynamics, *J. Lumin*., 207(2019), 169-176.
22. Z. S. Wang, H. Kawauchi, T. Kashima, H. Arakawa, Significant influence of TiO_2 photoelectrode morphology on the energy conversion efficiency of N719 dye-sensitized solar cell, *Coord. Chem. Rev*., 248(2004), 1381-1389.
23. S. H. Kang, J. Y. Kim, H. S, Kim, H. D. Koh, J. S. Lee, Y. E Sung, Influence of light scattering particles in the TiO_2 photoelectrode for solid-state dye-sensitized solar cell, *J Photochem. Photobiol. A: chem*., 200(2008), 294-300.
24. S. Ito, M. Nazeeruddin, P. Liska, P. Comte,R. Charvet, P,Péchy, M, Jirousek, A. Kay, S. Zakeeruddin, M. Grätzel, Fabrication of screen-printing pastes from TiO_2 powders for dye-sensitised solar cells, *Prog. Photovolt. Res. Appl.*, 14(2006), 589-601.
25. Y, Qiu, W. Chen, S. Yang, Double-layered photoanodes from variable-size anatase TiO_2 nanospindles: A candidate for high-efficiency dye-sensitized solar cells, *Angew Chem. Int. Ed*., 49(2010), 3675-3679.
26. M. Ranjbar, S. A. Mozaffari, E. Kouhestanian, H. Salar Amoli, Sonochemical synthesis and characterization of a Zn(II) supramolecule, bis(2,6

diaminopyridinium)bis(pyridine-2,6-dicarboxylato)zincate(II), as a novel precursor for the ZnO-based dye sensitizer solar cell, *J. Photochem. Photobiol. A: Chem*., 321(2016), 110–121.
27. B. O'Regan. M. Grätzel, A low-coat, high-efficiency solar cell based on dye-sensitized colloidal TiO_2 film. *Nature*, 353(1991), 737-739.
28. W. C. Chang, C. H. Lee, W. C. Yu, C. M. Lin, Optimization of dye adsorption time and film thickness for efficient ZnO dye-sensitized solar cells with high at-rest stability, *Nanoscale Research Letters*, 7(2012), 688-697.
29. S. Ito, T. Murakami, P. Comte, P. Liska, C. Grätzel, M. Nazeeruddin, M. Grätzel, Fabrication of thin film dye sensitized solar cells with solar to electric power conversion efficiency over 10%, *Thin Solid Films*, 516(2008), 4613-4619.
30. N. Tounsi, M. M. Habchi, Z. Chine, A. Rebey, B. E. Jani, Optical properties study of In.08Ga.92As/GaAs using spectral reflectance, photoreflectance and near-infrared Photoluminescence, *Superlattice. Microstruct*., 59(2013), 133-143.
31. Q. Zhang, G. Cao, Hierarchically structured photoelectrodes for dye-sensitized solar cells, *J. Mater. Chem*., 21(2011), 6769-6774.
32. S. A. Mozaffari, M. Ranjbar, E. Kouhestanian, H. Salar Amoli, M. H. Armanmehr, An investigation on the effect of electrodeposited nanostructured ZnO on the electron transfer process efficiency of TiO_2 based DSSC, *Mater. Sci. Semicon. Proc*., 40(2015), 285-292.
33. B. Tan, Y.Y. Wu, Dye-sensitized solar cells based on anatase TiO_2 nanoparticle/nanowire composites, *J. Phys. Chem. B*, 110(2006), 15932-15938.
34. B. Lee, D. K. Hwang, P. Guo, S. T. Ho, D. B. Buchholtz, C. Y. Wang, R. P. H. Chang, Materials, interfaces, and photon confinement in dye-sensitized solar cells, *J. Phys. Chem. B*, 114(2010), 14582-14591.
35. S. Khadtarea, A. S. Ansari, H. M. Pathan, S. H. Hana, K. M. Mahadevan, S. D. Mane, C. Bathula Silver nanoparticles loaded ZnO photoelectrode with Rose Bengal as a sensitizer for dye sensitized solar cells, *Inorg. Chem. commun*., 104(2019), 155-159.
36. S. Khadtare, A. S. Bansode, V. L. Mathe, N. K. Shrestha, C. Bathula, S. H. Han, H. M. Pathan, Effect of oxygen plasma treatment on performance of ZnO based dye sensitized solar cells, *J. Alloys and Compd*., 72415(2017), 348-352.
37. S. Khadtare, A. Ware, S. A. S. Gawali, S. R. Jadkar, H. M. Pathan, S. S. Pingale, Dye sensitized solar cell with lawsone dye using ZnO photoanode: experimental and TD-DFT study, *RSC Adv.*, 5(2015), 17647-17652.
38. P. Du, L. Songa, J. Xiong, N. Li, Z. Xi, L. Wang, D. Jin, S. Guob, Y. Yuan, Coaxial electrospun TiO_2/ZnO core–sheath nanofibers film: Novel structure for photoanode of dye-sensitized solar cells, *Electrochim. Acta*, 78(2012), 392-397.
39. S. H. Kang, J. Y. Kim, Y. Y. Kim, H. S. Kim, Y. E. Sung, Surface modification of stretched TiO_2 nanotubes for solid-state dye-sensitized solar cells, *J. Phys. Chem. C*, 111(2007), 9614-9623.
40. S. A. Mozaffari, R. Rahmanian, M. Abedi, H. Salar Amoli, Urea impedimetric biosensor based on reactive RF magnetron sputtered zinc oxide nanoporous transducer, *Electrochim. Acta*, 146(2014), 538-547.
41. S. A. Mozaffari, H. Salar Amoli, S. Simorgh, R. Rahmanian, Impedimetric thiourea sensing in copper electrorefining bath based on DC magnetron sputtered nanosilver as highly uniform transducer, *Electrochim. Acta*, 184 (2015) 475-482.
42. R. Rahmanian, S. A. Mozaffari, Electrochemical fabrication of ZnO-polyvinyl alcohol nanostructured hybrid film for application to urea biosensor, *Sensor Actuator B: chem*., 207(2015), 772-787.
43. F. F. Santiago, J. Bisquert, E. Palomares, L. Otero, D. Kuang, S. M. Zakeeruddin, M. Grätzel, Correlation between photovoltaic performance and impedance spectroscopy of dye-sensitized solar cells based on ionic liquids, *J. Phys. Chem. C*, 111(2007), 6550-6560.
44. J. Bisquert, F. F. Santiago, I. M. Ser, G. G. Belmonte, S. Gimenez, Electron lifetime in dye-sensitized solar cells: Theory and interpretation of measurements, *J. Phys. Chem. C*, 113(2009), 17278-17290.
45. R. J. Jennings, F. Li, Q. Wang, Reliable determination of electron diffusion length and charge separation efficiency in dye-sensitized solar cells, *J. Phys. Chem. C*, 114(2010), 14665–14674.
46. Q. Wang, S. Ito, M. Grätzel, F. F. Santiago, I. M. Sero, J. Bisquert, T. Bessho, H. Imai, Characteristics of high efficiency dye-sensitized solar cells, *J. Phys. Chem. B*, 110(2006), 25210-25221.
47. P. T. Hsiao, Y. L. Tung, H. Teng, Electron transport patterns in TiO_2 nanocrystalline films of dye-sensitized solar cells, *J. Phys. Chem. C*, 114(2010), 6762-6769.

How to cite this article:
E. Kouhestanian, M. Ranjbar, S. A. Mozaffari, H. Salaramoli, Investigating the Effects of Thickness on the Performance of ZnO-Based DSSC., *Prog. Color Colorants Coat*., 14 (2021), 101-112.